LASER MODIFICATION OF SURFACE PROPERTIES OF TI BASED COMPOSITES PREPARED VIA POWDER METALLURGY

RICHARD ANTALA[1], PETER SUGAR[1], JAROSLAV KOVACIK[2], JANA SUGAROVA[1], FILIP FERENCIK[3]

[1]Institute of Production Technologies, Faculty of Material Science and Technology, Slovak University of Technology, Trnava, Slovakia

[2]Institute of Materials and Machine Mechanics, Slovak Academy of Sciences, Bratislava, Slovakia

[3]Advanced Technologies Research Institute, Faculty of Material Science and Technology, Slovak University of Technology, Trnava, Slovakia

DOI: 10.17973/MMSJ.2025_06_2025052

richard.antala@stuba.sk

The study deals with the evaluation of the laser-modified surfaces of the progressive Ti-based composite materials intended for dental implantology applications. Two powder metallurgy-processed experimental materials, namely Ti-TiB_2 composite produced by the Spark Plasma Sintering (SPS) method and Ti-graphite composite produced by the Hot Vacuum Pressing (HVP) method, were investigated. The surface treatment of composites was carried out by nanosecond laser micromachining in atmospheric air, O_2 and Ar gas environments at various flow rates. The influence of laser micromachining on the relationship between surface morphology, wettability and chemical composition has been experimentally investigated via contact angle (CA) measurement using the sessile drop technique, SEM and EDS analysis. The sufficient surface structures with increased hydrophilicity were successfully prepared via laser modification technique in air on Ti-TiB_2 composite.

KEYWORDS

laser machining, powder metallurgy, Ti-TiB_2, Ti-graphite, wettability, chemical composition

1 INTRODUCTION

The development of materials that are biologically compatible with human tissue remains an ongoing challenge in contemporary implantology practice. Generally, metal-based implants should fulfil several functional properties, such as excellent biocompatibility combined with suitable mechanical properties and good corrosion and wear resistance, to function safely and maintain their performance over the longest possible time period.

Nowadays, many authors refer to titanium as the metal that meets these criteria and, along with its alloys and composites, represents one of the most commonly used medical materials in orthopaedic and dental implantology [Rossi 2008]. Considering the importance of the osseointegration process, i.e., the direct connection between the implant surface and the patient's body, various methods of modifying titanium implant surfaces have been developed to achieve better biomechanical conditions at the implant-tissue interface. Compared to the other dental implant surface modification technologies, such as etching, sandblasting or anodizing, the laser micromachining technology configured with pulse lengths ranging from ms to fs is considered one of the most versatile, cost-effective, and reliably reproducible methods for modifying Ti-based dental implants [Sirdeshmukh 2023, Tzanakakis 2021].

By focusing a laser beam, it is possible to induce melting and partial or complete evaporation of the irradiated surface, resulting in micro- and nanogeometric surface structures with topography, morphology, and chemical composition that enhance the surface's biocompatible, bioactive, and antibacterial properties [Bressel 2017, Eghbali 2021, Faeda 2009, Souza 2019]. For instance, surfaces with roughness parameter Ra values of 1 to 2 μm have a positive impact on the differentiation of osteoblasts, the cells forming a bone [Wennerberg 2009, Schnell 2019]. In addition, it is assumed that a laser-modified surface should be hydrophilic with increased surface energy and a negative surface charge, which helps to enhance the adsorption and orientation of individual proteins and mineral phases from the blood [Sirdeshmukh 2023].

The chemical nature of the surface layer also plays a crucial role in the success of osseointegration, as the high reactivity of titanium allows the implant surface to be enriched with biologically beneficial products from the surrounding atmosphere. Laser oxidation helps reinforce the naturally occurring passive layer composed predominantly of TiO_2 particles, which can improve biological, optical, and tribological properties [Zeng 2020]. Especially, the presence of oxide layers based on anatase and rutile is responsible for improved biocompatibility, bioactivity, and the antibacterial effects of implants [Medvids 2021]. For comparison, the process of laser irradiation in an Ar environment allows the formation of a homogeneous, surface layer without defects or cracks, thereby achieving good tribological properties with [Gao 2022].

Nonetheless, the disadvantage of Ti is its relatively high Young's modulus compared to bone tissue [Yoganandam 2020]. To eliminate uneven stress distribution on the surrounding bone tissue, also called the "stress shielding effect", great attention is focused on the development of new types of technologies inducing structures with a higher level of porosity. One of the ways to reach this goal is the production of implants using cost-effective powder metallurgy processes [Makau 2013].

2 MATERIALS AND METHODOLOGY OF EXPERIMENT

Two newly developed lightweight porous Ti composites intended for dental implant applications were prepared via different powder metallurgy production strategies.

Firstly, the Ti-TiB_2 composite was prepared by the Spark Plasma Sintering (SPS) of the CP HDH Ti powder with a purity of 99.40% (Kimet Special Metal Precision Casting Co., Ltd., China) and 5 vol. % of TiB_2 angular-shaped powder of 99.50 % purity (Sigma Aldrich, Germany) (Figure 1a).

Secondly, the Ti-graphite composite material consists of CP HDH titanium powder (Kimet Special Metal Precision Casting Co., Ltd., China) with a purity of 99.40% (particle size up to 32 μm, sharp, fragment-like shape) and 15 vol. % graphite flakes (Figure 1c) of 99.90% purity (particle size up to 16 μm) was prepared applying cold isostatic pressing (CIP) at a pressure of 200 MPa and hot vacuum pressing (HVP) by pressure of 500 MPa at a temperature of 450 to 470 °C.

Material	Chemical composition (wt. %)			
	Ti	O	C	B
Ti-TiB$_2$	86.6	6.0	4.6	2.7
Ti-Graphite	86.4	5.5	8.1	-

Table 1. Chemical composition of samples in the as-received state

Material	Contact angle (°)	Density (g.cm^{-3})	Porosity (%)	H_{IT} (GPa)	E_{IT} (GPa)
Ti-TiB$_2$	80.16	4.49	0.5	5.11	142.98
Ti-Graphite	65.10	4.15	2.44	3.31	96.83

Table 2. Selected properties of the experimental samples in the as-received state (H_{IT} – hardness, E_{IT} – Young's modulus by nanoindentation)

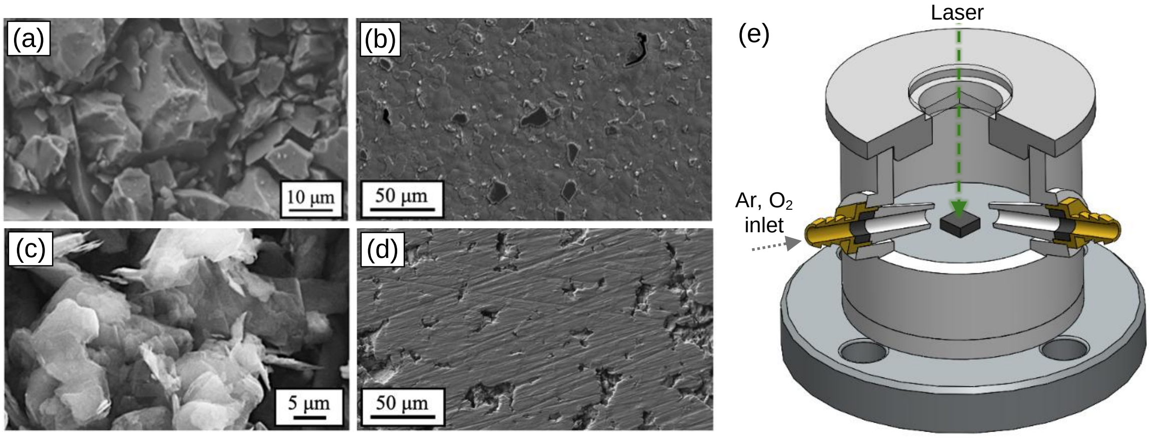

Figure 1. Sample preparation: a) TiB$_2$ powder, b) Ti-TiB$_2$ composite, c) graphite flakes, d) Ti-graphite composite, e) shielding chamber for laser micromachining

The surface modification in this study was carried out on a 5-axis machining centre Lasertec 80 Shape (DMG Mori GmbH, München, Germany), utilising the nanosecond Yb-doped fibre laser working with a constant pulse duration of 120 ns at 1064 nm wavelength and constant laser spot diameter of 50 µm. Prior to the machining process, the samples were ground with P600 and P1200 Buehler CarbiMet emery papers, cleaned with distilled water and ethanol and subsequently dried with a stream of hot air. Five groups of experiments were conducted using processing parameters that are depicted in Table 3.

The variables were a machined material type, a total amount of heat delivered to the irradiated area – transferred energy (E_T), type of assistance gas and its flow rate. The transferred energy E_T was calculated according to the equation (1), which comprises pulse energy E_P, laser spot diameter D, pulse-to-pulse distance D_L, and trace displacement D_T.

$$E_T = E_P \times \left(D^2/(D_L \times D_T)\right) \quad (1)$$

A pulse frequency (f) of 20 kHz, a track displacement (D_T) of 10 µm, a crosshatching strategy of two perpendicular layers, and a 1 µm depth of ablated layers were kept constant for all experimental surfaces of rectangular shape with dimensions of 5 x 5 mm x 3 µm.

Samples machined in Ar and O_2 gas atmospheres were placed inside of an experimental shielding chamber with a constant flow of gas through two inlet channels, as is shown in Figure 1e. Inner diameter of gas inlets is 6 mm and the time of gas inflow started 1 minute before laser irradiation.

Material	Sample	E_T (mJ)	E_P (mJ)	D_L (µm)	Gas	Flow rate (l.min^{-1})
Ti-TiB$_2$	B0A	0.5	0.2	100	Air	-
	B1A	1	0.2	50		
	B2A	2	0.8	100		
	B0Ar2	0.5	0.2	100	Ar	20
	B1Ar2	1	0.2	50		
	B2Ar2	2	0.8	100		
	B1Ar1	1	0.2	50	Ar	10
	B1Ar2		0.2	50		20
	B1Ar3		0.2	50		30
	B0O2	0.5	0.2	100	O_2	20
	B1O2	1	0.2	50		
	B2O2	2	0.8	100		
	B1O1	1	0.2	50	O_2	10
	B1O2		0.2	50		20
	B1O3		0.2	50		30
Ti-Graphite	G0Ar2	0.5	0.2	100	Ar	20
	G1Ar2	1	0.2	50		20
	G2Ar2	2	0.8	100		20

Table 3. Experimental design

To assess the wettability changes, the See System E goniometer (Advex Instruments, s. r. o., Brno, Czech Republic) was utilised for the static contact angle (CA) measurement before machining, 24 hours and 30 days after modification. The measurements were performed with three repetitions for each experimental surface using the deionised water with a droplet volume of 5 µL. Between each measurement, samples were cleaned with ethanol and dried under ambient air.

SEM analysis with a high-resolution scanning electron microscope TESCAN SOLARIS X (TESCAN ORSAY HOLDING, a. s., Brno, Czech Republic) was utilised to examine surface morphology changes. Laser-machined surfaces were analysed in secondary electron imaging mode with I = 1.0 nA, U = 20 keV and working distance WD = 5 mm at magnification ranging from 500 to 5000×. Chemical imaging of surfaces was performed via EDS map analysis with the Oxford Ultim Max65 EDS detector (Oxford Instruments, Abingdon, UK) at 1000× magnification under the same conditions.

3 RESULTS AND DISCUSSION

3.1 Surface morphology analysis

Major morphological differences were observed on surfaces modified by applying different transferred energy levels of laser irradiation, as can be seen in Figure 2a, 2b, and 2c at 1000× magnification, independently of the type of processing gas. Different results in surface morphology depending on the gas type can be observed at 3000× magnification (Figure 2d-i).

In terms of specific effects of laser beam parameters, the lowest level of transferred energy, 0.5 mJ (Figures 2d, 2g), given by the highest pulse distance D_L = 100 µm and lowest pulse energy E_P = 0.2 mJ, formed remelted isotropic surface morphology with visible craters after subsequent laser beam pulses. In contrast, an energy level of 1 mJ (Figures 2e, 2h) resulted in the formation of relatively "less separated" morphology due to shorter distances between adjacent laser spots (D_L = 50 µm) at the same level of pulse energy E_P = 0.2 mJ. The prominent effect on surface morphology was the increase of E_T to a level of 2 mJ (Figures 2f, 2i). The combination of a higher energy per pulse (E_P = 0.8 mJ) and prolonged pulse-pulse distances (D_L = 100 µm) helped to induce deep craters with the combination of micro- and sub-microgeometric structures on surface B2A (Figure 2f) and B2O2 (Figure 2i). This effect seems to be slightly diminished during irradiation of surface B2Ar2 in an Ar atmosphere (Figure 3c).

Laser machining in an O_2 atmosphere seems to induce more evident surface cracking compared to the processing in air or Ar at the same E_T level (Figure 2e-f).

In addition, the presence of Ar seems to induce higher material spattering within adjacent overlapping pulses compared to air (Fig. 2e) and O_2 atmosphere (Fig. 2h), where an increased presence of clearly defined, separate globules of resolidified material can be observed (Fig. 3b). In contrast, the highest value of E_T = 2 mJ (Fig. 3c) was accompanied by the presence of less spattered material and a smoother crater surface, which may be related to the less prominent hydrodynamic effects in the melt pool due to the inertness of Ar.

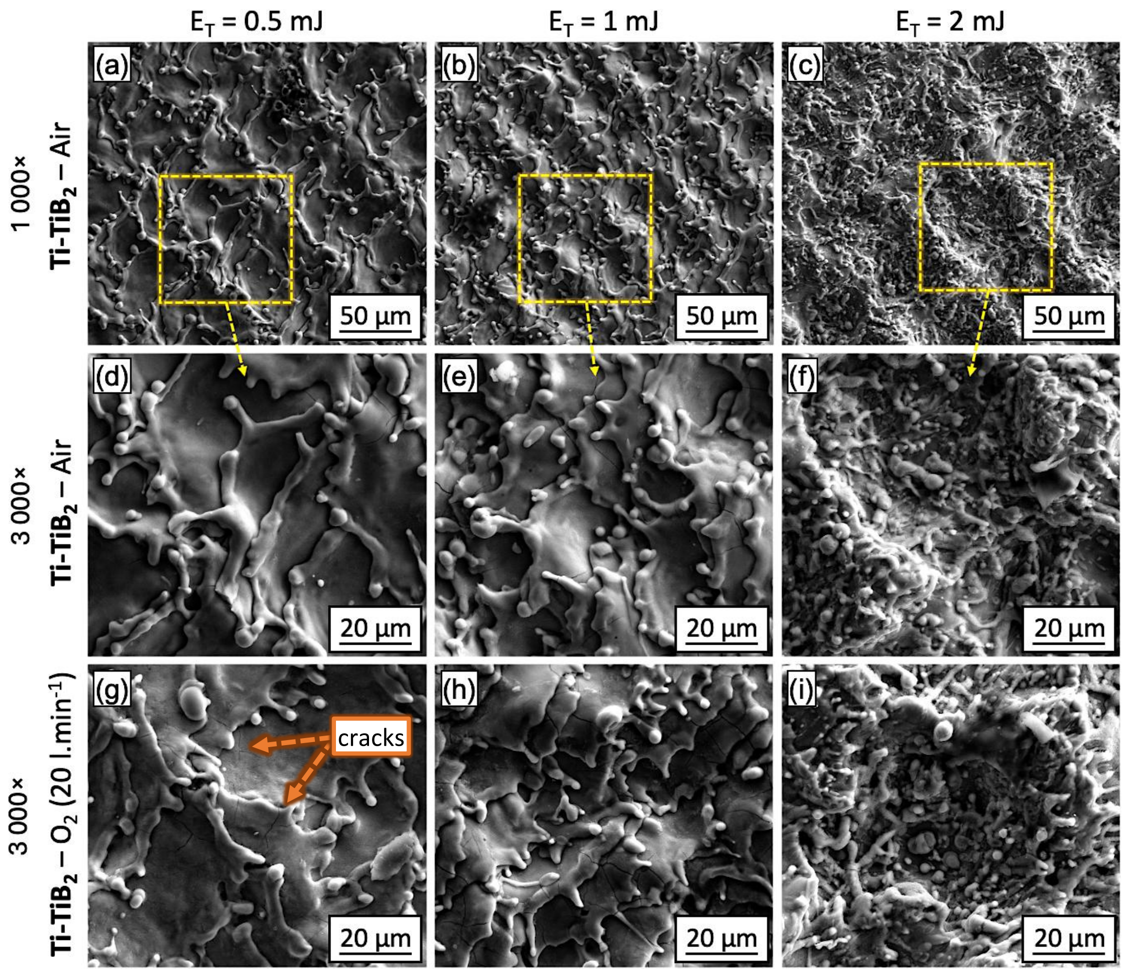

Figure 2. Ablated surfaces of Ti-TiB$_2$: a) B0A, b) B1A, c) B2A (1000×mag.) d) B0A, e) B1A, f) B2A (3000×mag.) g) B0O2 h) B1O2 i) B2O2 (3000×mag.)

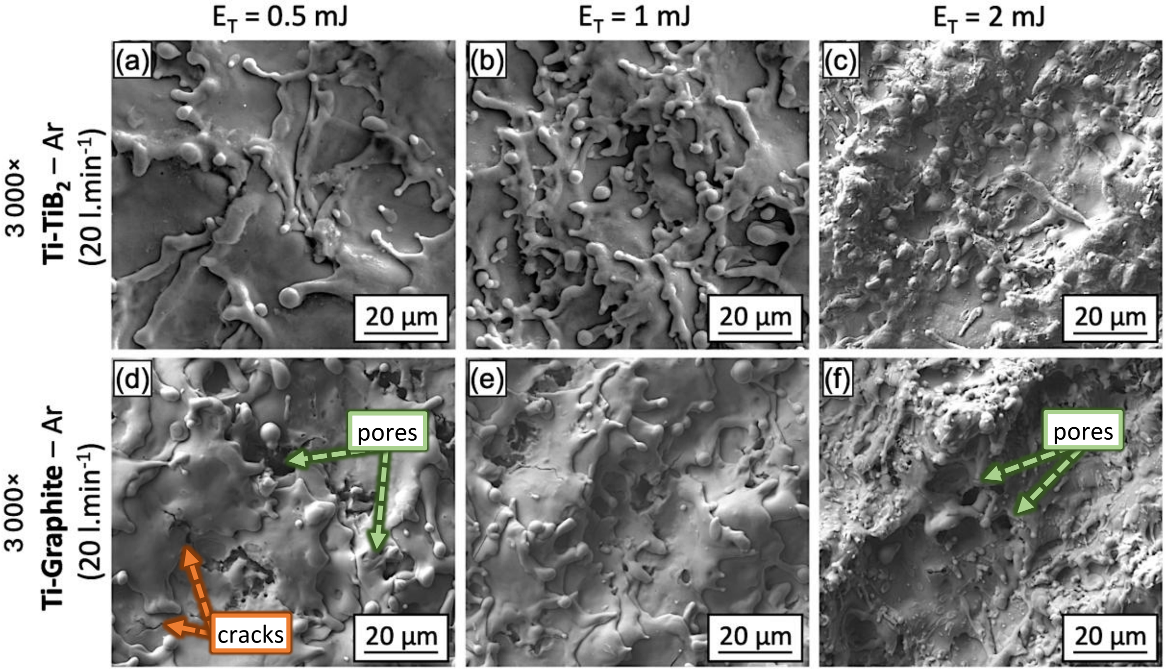

Figure 3. Ablated surfaces of Ti-TiB_2 and Ti-Graphite: a) B0Ar2, b) B1Ar2, c) B2Ar2, d) G0Ar2 e) G1Ar2 f) G2Ar2 (3000×mag.)

A similar effect can be observed on the irradiated surface of Ti-Graphite G2Ar2 (Figure 3f), which is characterized by the higher porosity compared to the Ti-TiB_2. Due to the 2.44% porosity of the Ti-Graphite, an increased presence of pores after laser modification can be seen in the case of all the samples prepared in an Ar atmosphere (Figure 3d-f). Interestingly, surfaces of Ti-Graphite ablated in Ar exhibited an increased cracking near pores, whereas in the Ti-TiB_2 samples, the Ar environment suppressed their formation, probably due to small pore size (from 0.5 to 1.5 µm). Pores in Ti-Graphite have ambiguous shape, due to the different powder metallurgy method (Fig. 1d). It can be concluded that the Ar environment helped to successfully prevent the formation of surface cracking on Ti-TiB_2 at either various energy levels and flow rates (Figures 4c, d, e). In the case of air atmosphere (Figure 4a), the presence of a small number of relatively long but narrow cracks can be observed.

The cracks coalesce into crack networks with increasing oxygen flow velocity (Figure 4f).

Prominent change in surface integrity was captured at the highest value of O_2 flow rate of 30 l.min^{-1}, when the topmost surface layer was formed of flaked, incoherent oxidic structure. An oxygen concentration of 43.6 at.% (Table 5) on surface B1O3 (Figure 4g) suggests potential presence of Ti_3O_2 or TiO phases after Ti-TiB_2 material resolidification.

3.2 Surface wettability evaluation

Obtained results from static contact angle analysis are summarised in Table 4 and Figures 5 and 6. In terms of resultant biocompatibility of Ti-TiB_2, laser surface modification helped to induce a hydrophilic surface state within the first 24 hours (Figure 5a, Figure 6a,b), that greatly decreased with time.

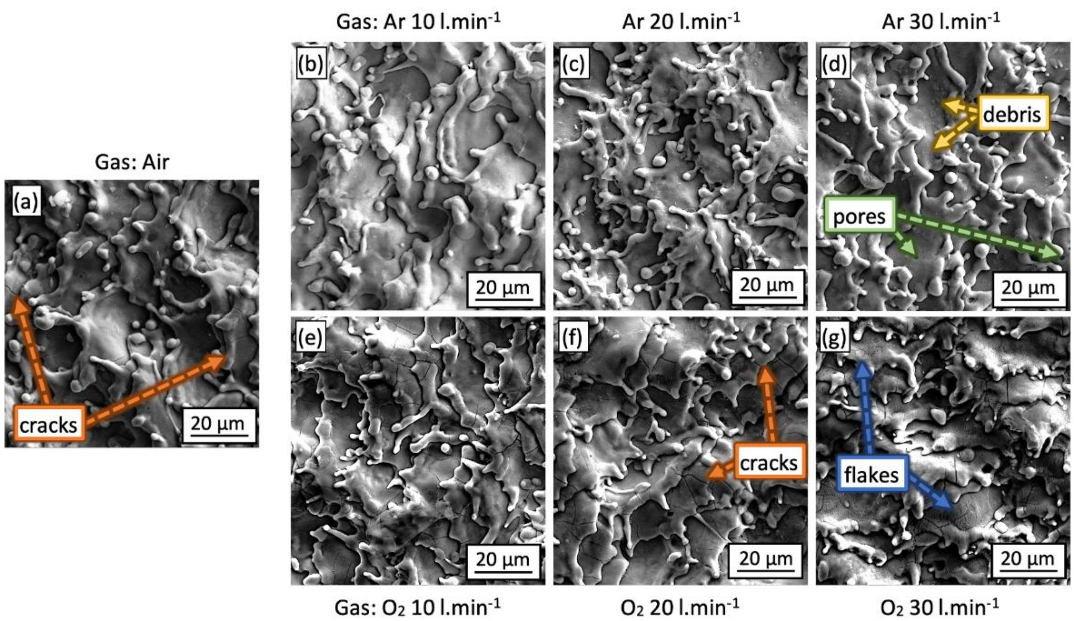

Figure 4. Ablated surfaces of Ti-TiB_2: a) B1V; b) B1Ar1; c) B1Ar2; d) B1Ar3; B1O1; f) B1O2; g) B1O3 (3000×mag.)

Material	Sample identification	1 day after ablation		30 days after ablation	
		CA (°)	SD	CA (°)	SD
Ti-TiB2	B0A	46.48	2.63	63.54	1.80
	B1A	38.81	2.44	51.27	3.41
	B2A	32.54	2.56	40.45	1.65
	B0Ar2	57.48	0.92	69.45	3.90
	B1Ar2	49.92	0.75	56.14	7.07
	B2Ar2	64.69	1.90	92.38	4.36
	B1Ar1	47.25	3.56	43.82	0.98
	B1Ar3	40.71	2.57	48.93	0.90
	B0O2	38.24	1.41	53.19	1.64
	B1O2	37.68	1.35	68.65	3.27
	B2O2	24.11	1.82	60.47	3.04
	B1O1	29.91	2.95	61.12	4.96
	B1O3	29.36	1.56	60.22	3.08
Ti-Graphite	G0Ar2	-	-	68.60	3.10
	G1Ar2	-	-	68.90	3.80
	G2Ar2	-	-	73.80	3.90

Table 4. Contact angles of laser machined surfaces

Expectedly, from the graph in Figure 5a is clear that, while the presence of atmospheric air and O_2 environments exhibited an expected decrease in CA with transferred energy alternation from 0.5 to 2 mJ, Ar seems to have an ambiguous effect on surface wettability. The increase in the amount of laser beam-induced energy during machining Ti-TiB_2 is often correlated with the increased concentration of oxidation products, which results in a CA reduction due to the polar effect of the induced oxidic layer. After machining of Ti-TiB_2 in an Ar shielding atmosphere, the surface morphology of B2Ar2 (Fig. 3c) seems to diminish the hydrophilic state due to the absence of polar oxygen-based products. Surfaces prepared in a Ar atmosphere seem to have generally the lowest wettability after 24 hours (Fig. 5a). In addition, the most dominant CA reduction after 30 days was captured on surface B2O2 (Fig. 2i) prepared in a O_2 atmosphere. This can be due to the surface aging effect, when the topmost polar oxidic layer loses its hydrophilicity due to the gradual adsorption of non-polar hydrocarbons and organic molecules.

As can be seen in Figure 5b, a similar trend with decreased wettability was captured in the transferred energy transition from 1.0 to 2.0 mJ for both composites after machining in an Ar environment with a 20 $l.min^{-1}$ flow rate. The difference in surface wettability of both composites is significant only at the highest level of E_T = 2 mJ.

An increase of the Ar flow rate was expected to increase the contact angle due to the diminished oxidation, which was confirmed in the flow rate of 0 to 20 $l.min^{-1}$ (Figure 6a). The trend of surface ageing was significant on all surfaces except B1Ar1. In comparison, an increase of the O_2 flow rate was expected to increase wettability (reduce CA), which was confirmed, except for the surface B1O1 (Fig. 6b). The ageing-induced hydrophobicity of the laser-modified surface after 30 days was more prominent and statistically significant in all surfaces ablated in an O_2 atmosphere.

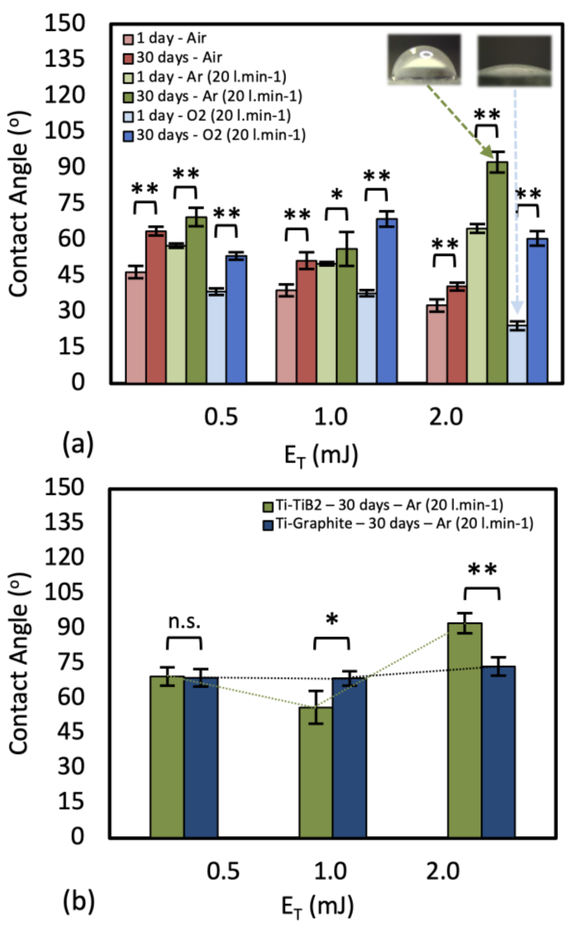

Figure 5. Effecf of E_T on CA: a) Ti-TiB_2 (Ar and O2 flow rate of 20 $l.min^{-1}$); b) Ti-TiB_2 and Ti-Graphite (Ar flow rate of 20 $l.min^{-1}$)

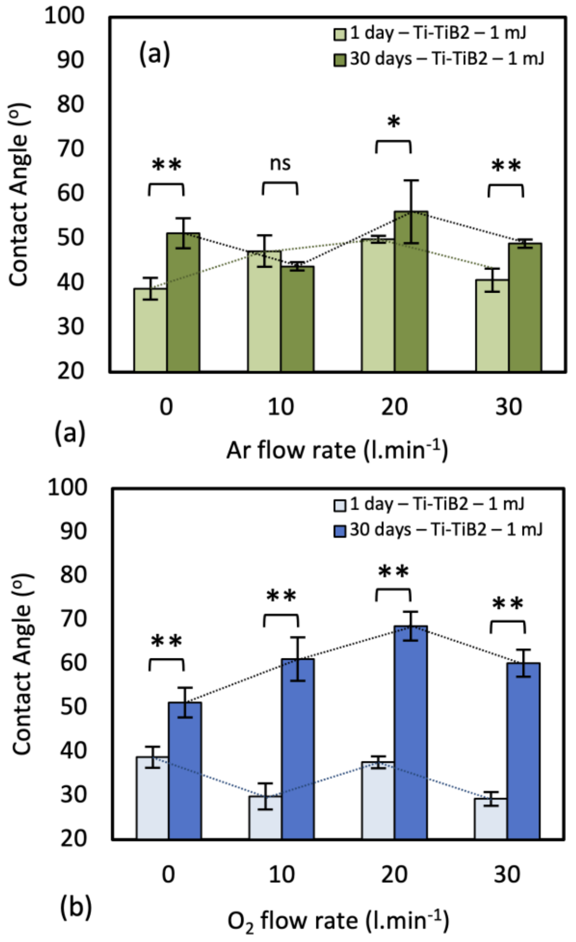

Figure 6. Effect of gas flow rate on CA of Ti-TiB_2 machined at E_T = 1 mJ: a) Ar, b) O_2

Material	Sample	Chemical composition (at. %)			
		Ti	O	C	B
Ti-TiB_2	B0A	49.1	30.1	17.0	3.7
	B1A	44.8	36.5	16.8	1.4
	B2A	41.3	40.0	16.8	1.9
	B0Ar2	46.1	34.0	18.4	1.3
	B1Ar2	45.0	34.7	18.2	1.8
	B2Ar2	45.0	34.4	17.8	2.6
	B1Ar1	44.1	32.3	21.8	1.6
	B1Ar3	46.9	32.5	15.8	4.0
	B0O2	42.1	39.9	15.9	2.2
	B1O2	35.5	42.2	20.9	1.4
	B2O2	33.9	46.7	15.3	4.1
	B1O1	45.0	40.9	12.8	1.3
	B1O3	35.3	43.6	20.2	0.8
Ti-Graphite	G0Ar2	59.4	23.8	16.8	-
	G1Ar2	64.2	15.2	20.6	-
	G2Ar2	47.9	35.1	17.0	-

Table 5. Chemical composition of laser machined surfaces

3.3 Analysis of chemical changes

The chemical composition of all machined surfaces is summarised in Table 5. The most dominant elements captured via EDS analysis were Ti, O, C and B, respectively. Expectedly, while the heat energy alternation in air decreased the concentration of Ti (Figure 7a), C (Figure 7c) and B, the presence of oxygen-based products was increased (Figure 7b). Oxygen concentration after laser modification in air was strongly positively correlated with E_T and increased wettability after 1 and 30 days ($r > 0.94$ in all cases). Expectedly, machining in Ar seems to diminish surface chemistry changes. The correlation between wettability and oxygen content is low in Ar ($r = 0.46$). The shift from the air to an O_2 atmosphere endorsed the formation of oxidation products by roughly 7 to 10 at.%, which may indicate the formation of the TiO phase. In this case, increased oxygen content is strongly positively correlated with both E_T ($r = 0.95$) and wettability after 1 day ($r = 0.95$).

Composition changes had a similar trend for both material groups (Figure 7d-f). Nonetheless, changes in the chemical composition seem to be more evident on Ti-Graphite, where the amount of oxygen increases ambiguously with E_T. The wettability on the Ti-Graphite surfaces decreases with oxygen content after both 1 and 30 days.

An increase of the O_2 flow, on the other hand, steadily increases the oxygen concentration with an unambiguous trend, which correlates with increased hydrophilicity after 1 day. This correlation was not evident after 30 days period (Figure 8b). The oxygen concentration decreases with Ar flow rate as expected.

3.4 Discussion

According to the authors [Faeda 2009, Souza 2019, Yang 2022], strong implant ability can be ensured by contact guidance phenomena, primarily due to the presence of suitable surface topography. Such surface structures were successfully prepared via the laser surface modification of Ti-TiB_2 in air using a transferred energy of 2 mJ due to the combination of altered surface area, highly hydrophilic state, and low presence of surface cracking compared to the same sample prepared in an O_2 atmosphere. The transferred energy alternation seems to be the crucial factor as well as the type of processing atmosphere.

The incorporation of O, H, and N into irradiated surfaces via diffusion is naturally increased above the temperature of 500°C. This is correlating with the increasing O_2 content as transferred heat energy is increased. Nonetheless, according to the Ti-O_2 phase diagram, a bioactive rutile phase of TiO_2 (more than 66.67 at.% of O_2) could not be expected on any of these surfaces [Rossi 2008, Zeng 2020]. Surface B2O2 prepared with the highest level of transferred energy in O_2 exhibited the highest wettability (CA = 24.11°) as well as the highest presence of oxygen (46.7 at.%) after irradiation. Compared to the inert Ar gas, the increase of the O_2 flow rate resulted in vivid cracking of remelted material with the presence of a flaked sub-oxidic structure, composed probably of Ti_3O_2 and TiO. Intensive surface cracking could be caused by the formation of hard martensitic α'-Ti phase during faster cooling time from β-Ti phase in O_2 rich atmosphere.

The Ar flow rate variation helped to produce a homogenous structure with reduced surface cracking, which is probably caused by better displacement of oxygen atoms from the irradiated area and better dissipating of heat due to its high heat capacity. which (Figure 4d) [Xie 2021].

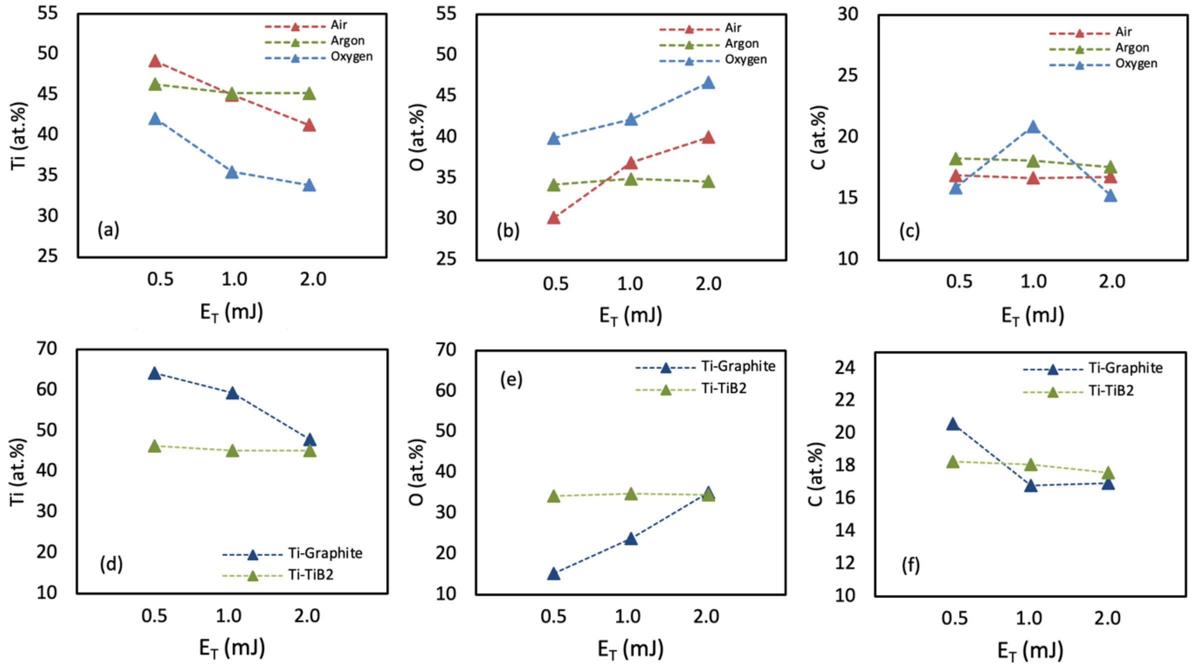

Figure 7. Effect of E_T on surface chemical composition: a – c) Ti-TiB_2 (Ar and O_2 flow rate of 20 l.min^{-1}), d – f) Ti-TiB_2 and Ti-Graphite (Ar flow rate of 20 l.min^{-1})

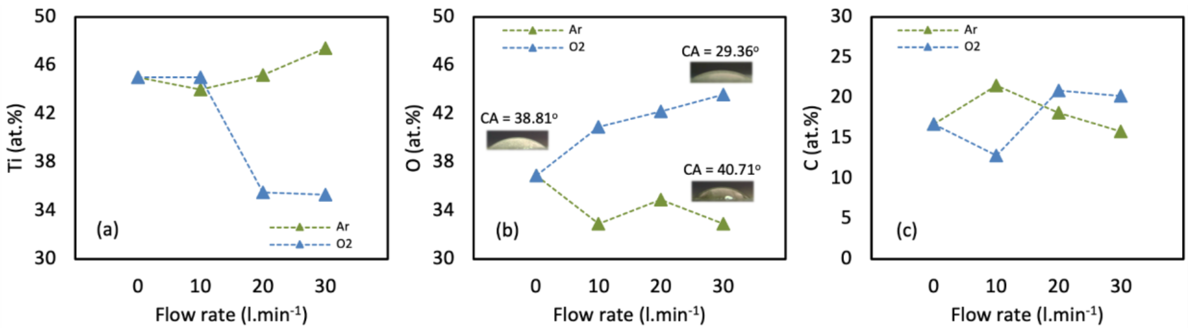

Figure 8. Effect of Ar and O_2 flow rate on Ti-TiB_2 chemical composition (E_T = 1 mJ)

A similar result of the increased wettability after laser irradiation with the amount of heat pulsed laser beam documented in this study was captured also by [Kasman 2023].

The observed decrease of the CA after irradiation could be explained via the Wentzel wetting state due to the presence of rugged surface topography that helps to better penetrate water droplets into pores and around surface irregularities, as well as via the presence of polar oxidic products, naturally helping with the adhesion of initial proteins [Rossi 2008]. Nonetheless, altered hydrophilicity gradually decreased after 30 days due to surface stabilization on all ablated surfaces. The hydrophilicity of surfaces is greatly correlated with transferred energy level and oxygen concentration. Different properties in terms of wettability were observed between the composites when higher energy values E_T = 2 mJ were applied. Since surface aging is more pronounced on oxygen rich surfaces, estimating the functional properties of the surface after 30 days has its limitations.

In addition, the presence of a hexagonal structure (C32) of the TiB_2 phase in Ti-TiB_2 has a similar thermal expansion as Ti, and its high resistance to oxidation could explain the less vivid chemical changes compared to the Ti-Graphite composite with prominent porosity [Ding 2015]. On the one hand, laser modification of the porous Ti-Grafite can help to achieve improved wettability and enhance surface topography, morphology or chemical state. Nonetheless, its porosity surprisingly acted as a stress concentrator during surface cooling in Ar. In comparison, the lower porosity of the Ti-TiB_2 composite helped to prevent surface cracking during laser machining, making it more favorable in terms of dental implant development by the nanosecond laser processing method.

CONCLUSION

Laser modification by pulsed laser beam was utilized to effectively influence the functional properties of new types of powder composites depending on the type of gaseous atmosphere.

The stable hydrophilic surface structure (CA = 32.54°) was successfully prepared via the laser modification technique in air on the surface of Ti-TiB_2 (B2A) with a transferred energy level of 2 mJ. In addition, surface wettability correlated with oxygen concentration due to transferred energy alternation.

While the fiber nanosecond laser used in this experiment seems to induce potentially suitable implant interfaces with sufficient surface morphology and strong hydrophilicity on both of the experimental Ti-based composites, new, lightweight, and porous powder metallurgy-prepared Ti-based composite materials can help to reduce the price and tailor the implant properties to the specific needs of the patient.

ACKNOWLEDGEMENT

The authors express their sincere thanks for the financial contributions. The authors declare no conflict of interest. The authors express their sincere thanks for the financial contributions, that supports this research, namely VEGA project 2/0054/23, the KEGA project 026STU-4/2023, and the project TIBLAS, solved under the STU Grand Scheme for Support of Young Researchers TIBLAS, solved under the STU Grand Scheme for Support of Young Researchers.

REFERENCES

[Rossi 2008] Rossi, S., Tirri, T., Paldan, H., Kuntsi-Vaattovaara, H., Tulamo, R. and Närhi, T. 2008 Peri-implant tissue response to TiO_2 surface modified implants Clin Oral Implants Res 19 348–55

[Sirdeshmukh 2023] Sirdeshmukh N and Dongre G 2023 Achieving controlled topography and wettability through laser surface texturing of Ti6Al4V for bioengineering applications Results in Engineering 17 100898

[Tzanakakis 2021] Tzanakakis, E.G.C, Skoulas, E., Pepelassi, E., Koidis, P. and Tzoutzas, I.G. 2021 The use of lasers in dental materials: A review Materials 14 (12): 3770

[Bressel 2017] Bressel T A B, De Queiroz J D F, Gomes Moreira S M, Da Fonseca J T, Filho E A, Guastaldi A C and Batistuzzo De Medeiros S R 2017 Laser-modified titanium surfaces enhance the osteogenic differentiation of human mesenchymal stem cells Stem Cell Res Ther 8 269

[Eghbali 2021] Eghbali, N., Naffakh-Moosavy, H., Sadeghi Mohammadi, S. and Naderi-Manesh, H. 2021 The influence of laser frequency and groove distance on cell adhesion, cell viability, and antibacterial characteristics of Ti-6Al-4V dental implants treated by modern fiber engraving laser Dental Materials 37 547–58

[Faeda 2009] Faeda, R. S., Tavares, H. S., Sartori, R., Guastaldi, A. C. and Marcantonio, E. 2009 Evaluation of titanium implants with surface modification by laser beam: biomechanical study in rabbit tibias Braz Oral Res 23 137–43

[Souza 2019] Souza, J. C. M., Sordi, M. B., Kanazawa, M., Ravindran, S., Henriques, B., Silva, F. S., Aparicio, C. and Cooper, L. F. 2019 Nano-scale modification of titanium implant surfaces to enhance osseointegration Acta Biomater 94 112–31

[Wennerberg 2009] Wennerberg, A. and Albrektsson, T. 2009 Effects of titanium surface topography on bone integration: A systematic review Clin Oral Implants Res 20 172–84

[Schnell 2019] Schnell, G., Staehlke, S., Duenow, U., Barbara-Nebe, J. and Seitz, H. 2019 Femtosecond laser nano/micro textured Ti6Al4V surfaces-effect on wetting and MG-63 cell adhesion Materials 12 13 2210

[Zeng 2020] Zeng C, Wen H, Zhang B, Sprunger P T and Guo S M 2020 Diffusion of oxygen and nitrogen into titanium under laser irradiation in air Appl Surf Sci 505 144578

[Medvids 2021] Medvids, A., Onufrijevs, P., Kaupužs, J., Eglitis, R., Padgurskas, J., Zunda, A., Mimura, H., Skadins, I. and Varnagiris S 2021 Anatase or rutile TiO2 nanolayer formation on Ti substrates by laser radiation: Mechanical, photocatalytic and antibacterial properties Opt Laser Technol 138 106898

[Gao 2022] Gao, X., Zhao, Y., Wang, M., Liu, Z. and Liu, C. 2022 Parametric Design of Hip Implant With Gradient Porous Structure Front Bioeng Biotechnol 10 1–15

[Yoganandam 2020] Yoganandam, K., Mohanavel, V., Vairamuthu, J. and Kannadhasan, V. 2020 Mechanical properties of titanium matrix composites fabricated via powder metallurgy method Mater Today Proc 33 3243–7

[Makau 2013] Makau, F. M., Morsi, K., Gude, N., Alvarez, R., Sussman, M. and May-Newman, K. 2013 Viability of Titanium-Titanium Boride Composite as a Biomaterial ISRN Biomaterials 2013 1–8

[Yang 2022] Yang, K., Shi, J., Wang. L., Chen, Y., Liang, C., Yang, L. and Wang, L. N. 2022 Bacterial anti-adhesion surface design: Surface patterning, roughness and wettability: A review J Mater Sci Technol 99 82–100

[Xie 2021] Xie, W., Quinn, J., Zhang, J., Carson, L. and Chan, C. W 2021 Control of laser-gas-material interactions to enhance the surface properties of NiTi for orthopaedic applications Surf Coat Technol 421 127403

[Kasman 2023] Kasman, Ş., Uçar, İ. C. and Ozan, S. 2023 Investigation of laser surface texturing parameters of biomedical grade Co-Cr-Mo alloy International Journal of Advanced Manufacturing Technology 125 4271–91

[Ding 2015] Ding H, Zhou G, Liu T, Xia M and Wang X 2015 Biotribological properties of Ti/TiB2 multilayers in simulated body solution Tribol Int 89 62–6

CONTACTS:

Richard Antala, Ing.; Sugár Peter, prof. Ing. CSc.; Sugarova Jana, doc. Ing. PhD.
Slovak University of Technology in Bratislava, Faculty of Material Science and Technology in Trnava
Institute of Production Technologies
Jana Bottu 25, 917 24 Trnava, Slovakia
richard.antala@stuba.sk; peter.sugar@stuba.sk; jana.sugarova@stuba.sk

Filip Ferencik, Ing.
Slovak University of Technology in Bratislava, Faculty of Material Science and Technology in Trnava
Advanced Technology Research Institute
Jana Bottu 25, 917 24 Trnava, Slovakia
filip.ferencik@stuba.sk

Jaroslav Kovacik, Ing. PhD.
Slovak Academy of Sciences
Institute of Materials and Machine Mechanics
Dubravska cesta 9/6319, 845 13 9, Bratislava, Slovakia
jaroslav.kovacik@savba.sk